SCANNING PROBE MICROSCOPY OF BIOMACROMOLECULES: NUCLEIC ACIDS, PROTEINS AND THEIR COMPLEXES

O.I. KISELYOVA, M.O. GALLYAMOV, N.S. NASIKAN and
I.V. YAMINSKY
*Chair of Polymer and Crystal Physics, M.V. Lomonosov Moscow State
University Vorobyevy Gory, Moscow, 119899, Russia*
O.V. KARPOVA, V.K. NOVIKOV
*Department of Virology, M.V. Lomonosov Moscow State
University Vorobyevy Gory, Moscow, 119899, Russia*

1. Introduction

After successful imaging of DNA biomacromolecules using scanning probe microscopy (SPM) (Bustamante et al., 1992) much progress was achieved in the visualization of their different morphological features in air and liquid environments: cruciforms, R-loops, etc. SPM gives an opportunity for real-time studies of conformational changes of DNA molecules induced by chemical reagents - formation of torroidal and rod-like structures. Recently, SPM has greatly assisted in the measurements of electrical conductivity of individual DNA molecules (Kasumov et al., 2001). SPM opens new possibilities in the study of single macromolecule micromechanics: rigidity, strength of chemical bond and adhesion.

Though, it is only in few cases that SPM permits to observe inner structure of protein molecules, it can still be used in advanced experiments for chemical sensing (Friorini et al., 2001), measurements of intermolecular forces, antigen-antibody reactions. Atomic force microscopy (AFM) gives new advantages over other high-resolution techniques in the observation of dynamic processes involving protein molecules: aggregation, crystallization and thin film formation. AFM was applied for the *in-situ* observation of lysozyme crystal growth. The defect structure, kinetics of kinks and step movement was studied; kinetic parameters (step and kink velocities, nucleation rate, etc.) were defined (Chernov et al., 1999).

The present paper is devoted to AFM of plant viruses. Most plant viruses are well ordered complexes of biomacromolecules: nucleic acids and proteins. From the structural viewpoint virus particles have the simplest organization compared to other organisms. Quantitative information on their mechanical properties will help to verify biomechanical models developed for these "simple" biological systems.

In this work we image, study and compare two well-studied RNA-containing viruses belonging to two different families: tobacco mosaic virus (TMV) from tobamovirus family and potato virus X (PVX) from the potex virus group. Virus particles of both species are composed of RNA wrapped into protein molecules. TMV particles are rod-

shaped, they look like rigid "sticks" (Knapp and Lewandowski, 2001), whereas PVX ones have elongated filamentous shape, are much softer and protein coverage is less dense. Here we make quantitative estimations of the rigidity of individual virus particles by means of AFM.

Traditionally when AFM is used for micro-mechanical measurements, the elasticity of materials is calculated on the basis of the information extracted from force curves (Radmacher et al., 1994). In our case, it was difficult to reliably maintain the probe over a single particle and we worked out and applied a different approach. The operation of AMF results in the 3D profile of the probe displacement, collected at constant probe-sample interaction force. The value of this force can be varied, which allows getting information about the elastic properties of the objects investigated. The probes impact on the sample leads to contact deformations (Drygin et al., 1998; Gallyamov et al., 2000), the value of which is determined by the applied force, elastic properties of the objects and the geometry of the contact area. For "soft" objects (polymer, biological ones) immobilized on a "rigid" substrate the consideration of probe-sample contact geometry allows to connect the dependency of deformation versus the applied force with elastic properties of the investigated objects.

2. Sample preparation

Purification of TMV and PVX particles was carried out as previously described by Drygin et al., (1998) and Atabekov et al., (2001) respectively. Mica, highly oriented pyrolitical graphite (HOPG) and aminopropylsilatran-treated mica (APS-mica) were used as substrates. In order to prepare APS-mica, freshly cleaved mica was incubated in the APS solution, rinsed in bidistilled water and dried (Shlyakhtenko et al., 1998). A 5-10 μl drop of the solution containing virus particles was placed onto the substrate, incubated for 5 minutes, rinsed with bidistilled water and dried. The average height of particles in each image was measured automatically using the software FemtoScan 001 (Filonov and Yaminsly, 1997).

3. Results and discussion

3.1. *IMAGING OF VIRUSES*

For AFM imaging TMV and PVX virus particles were applied on traditionally used substrates: graphite and mica. TMV particles adhered to both (Drygin et al., 1998), but the adsorption rate was higher on graphite surface (fig. 1 a). At the same time, TMV particles were more stable on mica substrate, which was used for contact mode experiments (data not shown). Interestingly, PVX particles did not adhere to mica and demonstrated no stability on graphite (Kiselyova et al., 2001). For their immobilization APS-treated mica (APS-mica) was applied. This substrate had previously been used in AFM experiments for nucleic acids immobilization (Shlyakhtenko et al., 1998). AFM images of PVX particles (fig. 1 b) show that their filamentous shape.
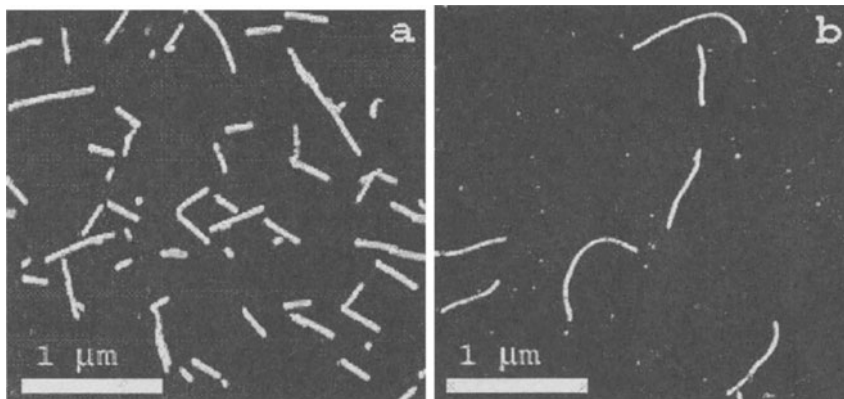
Figure 1. AFM images of (a) TMV particles on pure mica and (b) PVX particles on APS-mica obtained in contact mode

The height of particles revealed in tapping mode AFM images in was 13±2 nm, close to that provided by X-ray data reported by Varma et al., (1968) and particle's diameter measured by electron microscopy. Measurements of TMV particles height 18±2 nm gave good coincidence with conventional data as well (Knapp and Lewandowski, 2001). Distributions of particle's lengths revealed tail-to-tail aggregation effect (Drygin et al., 1998; Kiselyova et al., 2001).

In the next series of experiments PVX was subjected to RNase treatment. It is known that this procedure degrades the encapsidated RNA (Atabekov et al., 2001). Meanwhile, protein-protein interaction is so strong that it does not affect the integrity of virus particles. In AFM images RNase-treated particles looked the same and had the same dimensions as intact ones (fig. 2 a). Since TMV RNA is not destroyed by RNase treatment of TMV particles similar experiment was of no interest.
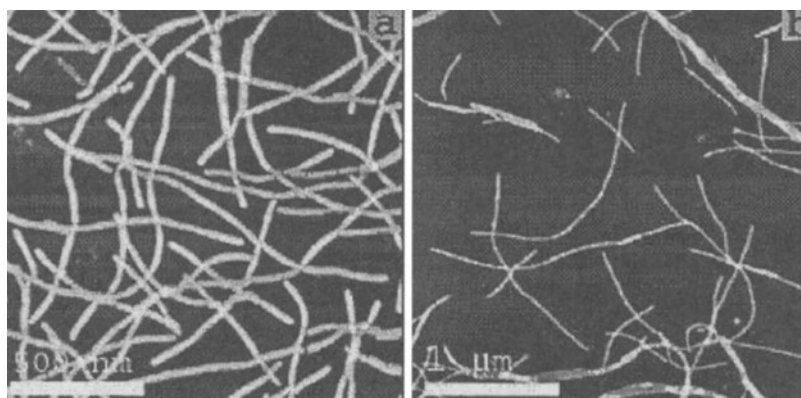

Figure 2. PVX particles subjected to treatments: (a) RNase treatment (b) – tripsin degradation.

Tripsin treatment of PVX degrades the 14-aminoasid N-terminus chain of PVX coat protein. This provokes particles side-to-side aggregation depicted in fig. 2 b.

Instability of PVX particles on HOPG yielded unexpected results. Intact virus particles were not observed, but considerably thinner structures (presumably viral RNA molecules) were revealed (fig. 3). RNA strands were seen as straight lines, their height was 0.55 ± 0.05 nm, the width measured at half height – 8 nm. Previously, for RNA molecules, observed in AFM on freshly cleaved mica surface, these parameters were found to be in the intervals of 0.3-1.5 nm and 10-15 nm respectively (Drygin et al., 1998).
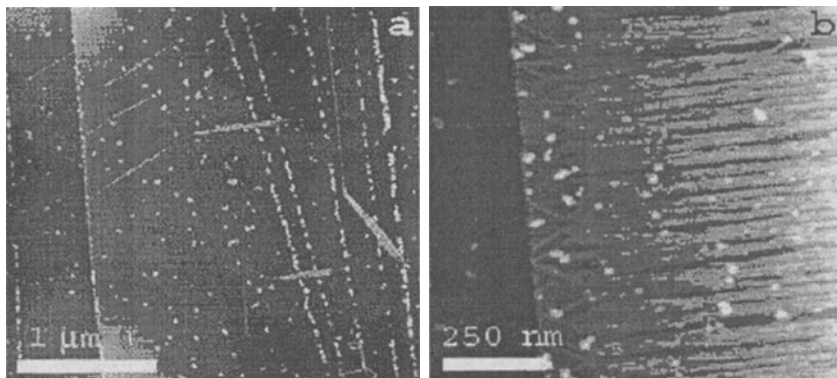

Figure 3. Decomposition of PVX particles on graphite substrate. Filaments are presumably RNA molecules unfolded and stretched on the crystalline lattice.

The apparent dimensions of RNA adsorbed on HOPG are closer to real RNA geometry, than those of mica-adsorbed RNA. We suppose that this difference is due to the well-known and widely discussed effect of thin water film, covering mica surface at ambient humidity (Guckenberger et al., 1994). The extended distribution of parameters for the RNA described by Drygin et al., (1998) can be presumably attributed to the fact that when adsorbed to mica, RNA has many bends and its secondary structure is not completely unfolded, whereas the molecules registered on HOPG are straightened.

The angles between adsorbed RNA molecules directions were multiple to 60°, which coincides with angles in HOPG crystalline lattice. This implies that substrate-RNA interaction was so strong that not only virus particles were decomposed, but the secondary structure of RNA was unfolded as well. RNA molecules tended to form flat parallel aggregates (fig. 3 b).

3.2. CALCULATION OF CONTACT DEFORMATION

Let's consider the contact area between an AFM probe tip and the investigated, specimen placed on a flat substrate surface. According to Hertz solution (Landau and Lifshitz, 1987), two bodies in contact, pressed by the force F, are deformed and brought towards each other by the distance h, the contact area no longer being a point but becoming a spot with a finite square S (fig 4.).
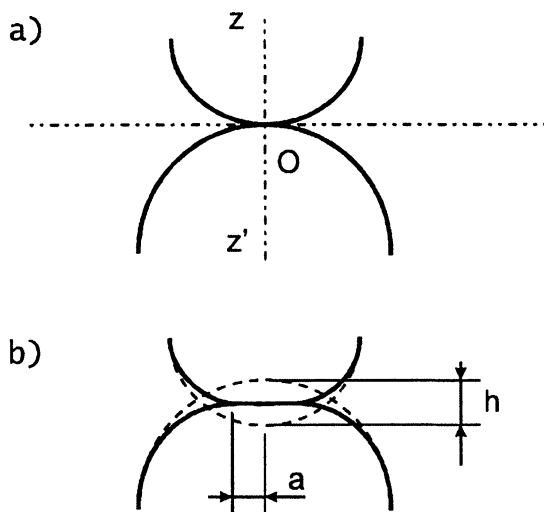
Figure 4. Contact deformation of two bodies. (a) – no compressing force, (b) compressing force applied.

The task analysis requires consideration of summarized curvature tensor of contact surfaces $\chi_{\alpha\beta}+\chi'_{\alpha\beta}$, which principle value A and B can be expressed in principle curvature radii of contact surfaces (Landau and Lifshitz, 1984). If the deformation is small compared to curvature radii, the contact area shape is an ellipse with semi axes a and b. These values and rapprochement h, are expressed in the implicit form using known task parameters: applied force F and contact geometry parameters A and B:

$$h = \frac{FD}{\pi} \int_0^\infty \frac{d\xi}{\sqrt{(a^2+\xi)(b^2+\xi)\xi}},$$

$$A = \frac{FD}{\pi} \int_0^\infty \frac{d\xi}{(a^2+\xi)\sqrt{(a^2+\xi)(b^2+\xi)\xi}}, \tag{1}$$

$$B = \frac{FD}{\pi} \int_0^\infty \frac{d\xi}{(b^2+\xi)\sqrt{(a^2+\xi)(b^2+\xi)\xi}}$$

D — being inverse effective elastic modulus of the contact area:

$$D = \frac{3}{4}\left(\frac{1-\sigma^2}{E} + \frac{1-\sigma'^2}{E'}\right), \tag{2}$$

where E and E' are Young's moduli and σ and σ' - Poisson's ratios for the probe and the sample materials, respectively.

In certain practically important cases equations (1) can be simplified and solved analytically. Since virus particles investigated have cylindrical shape the model to be considered is the model of spherical tip and cylindrical sample.

For the contact of a spherical probe with (radius R) and a surface of a cylinder (radius R') parameters A and B are expressed in the following form

$$A = \frac{1}{2}\left(\frac{1}{R} + \frac{1}{R'}\right), \quad B = \frac{1}{2R}. \tag{3}$$

Unfortunately, in this case the parameters of interest cannot be explicitly expressed from (1). Numerical solution yields three equations to be solved sequentially:

$$\frac{b^2}{a^2} = \frac{A}{B}\frac{K}{E} - \frac{A}{B} + \frac{K}{E},$$

$$b^3 = \frac{2FD}{\pi B}\frac{(K-E)}{\left(1 - \frac{a^2}{b^2}\right)} \tag{4}$$

$$h = \frac{2FD}{\pi b}K,$$

where $K \equiv K(\sqrt{1 - a^2/b^2})$, $E \equiv E(\sqrt{1 - a^2/b^2})$ — full elliptical integrals.

If the radius of the cylinder is less that the probe radius, (3) implies, that principle values of the summarized curvature tensor differ: $A > B$. Using (1), one can show that in this case $a < b$. If $a^2 \ll b^2$ equations (4) can be simplified, using a well known asymptotic for a full elliptical integral. Then, rapprochement h is expressed as follows:

$$h = \left(\frac{4}{\pi^2 C}\right)^{1/3}(C+1)B^{1/3}(FD)^{2/3} \tag{5},$$

parameter C depending on the ellipse parameters a and b:

$$C = \ln\left(\frac{4b}{a}\right) - 1 = \frac{Bb^2}{Aa^2} \tag{6}$$

Formula (6) yields numerical value of b/a and C, provided B/A is known. Numerical solution shows that typical values of C for many tasks lie in between 1 and 3.

3.3. EXPERIMENTAL DETERMINATION OF YOUNG'S MODULUS

The difference of formula (5) from Hook's law is the non-linear dependence of the deformation h versus the applied force. This is explained by the fact that the size of the contact area also depends on the applied force.

We studied the deformation of virus particles at different values of the force applied from the probe (figure 5 (a) for TMV, (b) for PVX) and revealed that it fits the "two thirds" dependency (compare to (5),

$$h \sim (FD)^{2/3} f(R, R') \qquad (7),$$

where f is the function of probe and the sample radii R and R' respectively.
Generally, three terms contribute to the reduction of sample height in the AFM image due to contact deformation:

$$\ddot{A}h_{\acute{O}} = \ddot{A}h_{probe/sample} + \ddot{A}h_{sample/substrate} - \ddot{A}h_{probe/substrate}$$

Where the second term is practically equal to the first one for small radii of the sample.

Thus, the measured height of virus particles H, can be found from the following formula:

$$H = H_0 - 2(FD)^{2/3} f(R, R'),$$

where H_0 is the height (diameter) of a non-deformed particle.

Since the value of Poisson's ratios for the used materials $\sigma^2 \ll 1$, Young's modulus for silicon $E \sim 10^{11}$ Pa, and for biological objects E can be estimated as $E \sim 10^9$ Pa and less, the equation (2) can be simplified to:
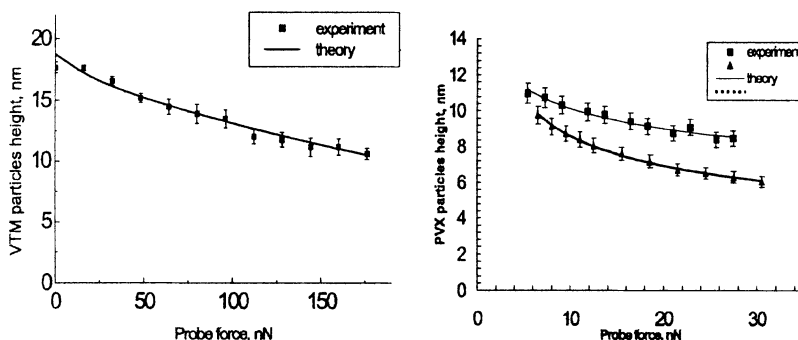

Figure 5. "Two thirds" dependency of particles' height versus the applied force.
(a) - TMV, (b) - PVX. In image (b) squares and continuous line correspond to intact particles, triangles and dotted line – to RNase-treated ones.

$$D \sim \frac{3}{4E} \qquad (8)$$

The approximation of experimental points by theoretical curve was performed using the least meant square method. Experimental errors were determined as standard deviations of average h values obtained from several AFM images. The obtained parameters yielded the coefficient D, then Young's modulus was found to be $E \sim 3 \cdot 10^9$ Pa for TMV particles and $E \sim 8 \cdot 10^8$ Pa for PVX ones. Previously, Young's modulus was measured alternatively, providing a very close value of $E \sim 1.1 \cdot 10^9$ Pa (Falvo et al., 1997). Thus, the obtained value for PVX is almost by the order of magnitude less than that for TMV. This explains the difference in the appearance of two virus's particles adsorbed on the substrate: PVX particles are curved whereas TMV one remain practically straight.

For RNase-treated PVX particles the dependency of deformation versus the applied force was more drastic than for intact ones (fig. 5 b). Let's remind that in tapping mode images intact and RNase-treated particles had the same dimensions. The deformation was so essential that could no longer be described by the Hertz model. These data imply that though visually PVX particles remained unchanged, their rigidity was lost after RNA disruption.

3.4. DEFORMATIONS OF VIRUS IN TAPPING MODE

Though lateral tip-sample forces are very small in tapping mode, the deformation of soft objects occurs nevertheless. In tapping mode the contact between the probe tip and the sample is temporary and the contact deformations cannot be calculated according to the above-mentioned procedure. Here we compare the apparent heights of PVX particles obtained in contact and tapping regimes and study the influence of cantilever oscillations parameters on the obtained data. PVX was chosen because it is "softer" and deformations are easier to register.

Vertical dimensions of PVX particles imaged in contact mode, the contact force being minimized, was 11.0 nm, i.e. 20% less than in tapping mode (13.5 nm), presumably due to stronger deformation of particles in the contact regime.

It was demonstrated that the apparent height of PVX particles depended on the aspect ratio A/A_0, (loaded versus free oscillation amplitude). Namely, the height reduced as the aspect ratio was decreased and therefore the effect of the probe was strengthened (fig. 6 a).

Height reduction by 15% was registered at the aspect ratio value of 0.5. It is noteworthy, that the deformation of the particles was absolutely reversible. Interestingly, the amplitude of cantilever's free oscillations also influenced the apparent height. Two-times increase of the amplitude from 15 to 30 nm reduced the obtained height by almost 30 % (fig. 6 b). These data show that one has to be very careful about choosing tapping mode parameters when quantitative measurements are performed.
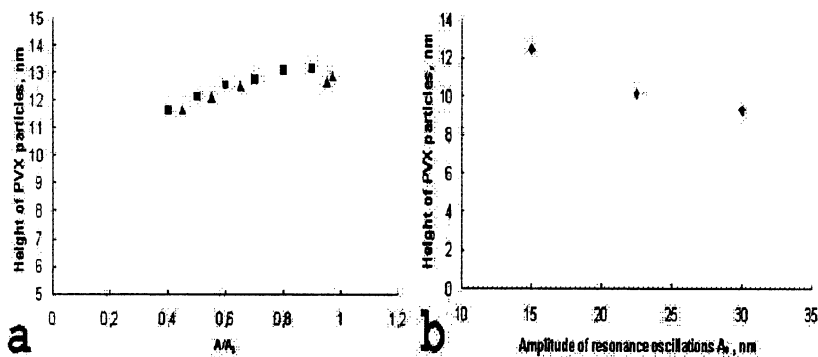
Figure. 6. The influence of tapping mode scanning parameters on PVX particles' height.
(a) height versus aspect ratio (A/A_0). Squares mark points obtained when reducing and triangles when increasing A/A_0.
(b) height versus free oscillations amplitude (A_0).

4. Conclusion

AFM can be successfully used as an imaging tool in descriptive virology. It observes virus morphology with subnanometer accuracy. It also presents direct data about mechanical properties of individual virus particles, which are not obtained in other high-resolution imaging methods. This is new information for biology and the way of its practical comprehension is to be developed. Still the demonstrated AFM method opens new opportunities in micromechanical measurements of different nanostructures in nanotechnological applications. Different virus particles may serve here as well-defined rigidity standards.

5. Acknowledgement

References

1. Atabekov, J.G., Rodionova, N.P., Karpova, O.V., Kozlovsky, S.V., Novikov, V.K., Arkhipenko, M.V. (2001), "Translational Activation of Encapsidated Potato Virus X RNA by Coat Protein Phosphorylation", Virology 286 (2), 466-474.
2. Bustamante, C., Vesenka, J., Tang, C.L., Rees, W., Guthold, M., and Keller, R. (1992), "Circular DNA Molecules Imaged in Air by Scanning Force Microscopy", Biochemistry, 31(1), 22-26.
3. Chernov, A.A., Rashkovich, L.N., Yaminsky, I.V., and Gvozdev, N.V. (1999), "Kink Kinetiks, Exchange Fluxes, 1D 'Nucleation' and Adsorption on the (010) Face of Orthorombic Lysozyme Crystals", Journal of Physics: Condensed Matter 11, 9969-9984.

4. Drygin, Yu.F., Bordunova O.A., Gallyamov M.O., and Yaminsky I.V. (1998), "Atomic Force Microscopy Examination of Tobacco Mosaic Virus and Virion RNA", FEBS Letters 425, 217–221.
5. Falvo, M.R., Washburn, S., Superfine, R., Finch, M., Brooks, F.P., Jr., Chi V., and Taylor R.M. (1997), "Manipilation of Individual Viruses: Friction and Mechanical Properties", Biophysical Journal 72, 1396-1403.
6. Filonov A.S., and Yaminsky, I.V. (1997), SPM control and image processing software,. Chichester: Advanced Technologies Center, Moscow.
7. Fiorini, M., McKendry, R., Cooper, M.A., Rayment, T., and Abell, Ch. (2001), "Chemical Force Microscopy with Active Enzymes", Biophysical Journal 80(5), 2471-2476.
8. Gallyamov, M.O., Drygin, Yu.F., and Yaminsky, I.V. (2000), "Atomic Force Microscopy Visualization of RNA and Ribonucleotides of Tobacco Mosaic Virus". Surface Investigation 15, 1127–1134.
9. Guckenberger, R., Heim, M., Cevc, G., Knapp, H.F., Wiegräbe, W., and Hillebrand, A. (1994), "Scanning Tunneling Microscopy of Insulators and Biological Specimens Based on Lateral Conductivity of Ultrathin Water Films", Science 266, 1538-1540.
10. Kasumov, A.Yu., Kociak, M., Guéron, S., Reulet, B., Volkov, V.T., Klinov, D.V., and Bouchiat, H. (2001), "Proximity-Induced Superconductivity in DNA", Science 291, 280-282.
11. Kiselyova, O.I., Nasikan, N.S., Yaminsky, I.V., and Novikov, V.K. (2001) "AFM Imaging of PVX Particles and PVX RNA", Physics of Low-Dimensional Structures 3/4, 167-174.
12. Knapp, E. and Lewandowski, D.J. (2001), "Tobacco Mosaic Virus Not Just a Single Component Virus Anymore", Molecular Plant Pathology, 2(3), 117-123.
13. Landau, L.D., and Lifshiz, E.M. (1987) Theoretical Physics, V. 7 (in Russian), Nauka, Moscow.
14. Radmacher, M., Fritz, M., Cleveland, J.P., Walters, D.A., and Hansma, P.K. (1994), "Imaging Adhesive Forces and Elasticity of Lisozyme Adsorbed on Mica with the Atomic Force Microscope", Langmuir 10, 3809-3814.
15. Shlyakhtenko, L.S., Potaman, V.N., Sinden, R.R. and Lyubchenko, Yu.L. (1998), "Structure and Dynamics of Supercoil-Stabilized DNA Crusiforms", Journal of Molecular Biology 280, 61-72.
16. Varma, A., Gibbs, A.J., Woods, R.D., and Finch, J.T. (1968), "Some Observations on the Structure of the Filamentous Particles of Several Plant Viruses", Journal of General Virology 2, 107-114.